Cement and Concrete Research 40 (2010) 1165–1174

Contents lists available at ScienceDirect

Cement and Concrete Research

journal homepage: http://ees.elsevier.com/CEMCON/default.asp

Modeling the degradation of Portland cement pastes by biogenic organic acids

Laurent De Windt [a,*], Philippe Devillers [b]

[a] Geosciences Dept., Ecole des Mines de Paris, Mines-ParisTech, 35 Rue St-Honoré, 77305 Fontainebleau, France
[b] Centre des Matériaux de Grande Diffusion, École des Mines d'Alès, 6 Av. de Clavières, 30319 Alès, France

ARTICLE INFO

Article history:
Received 4 September 2009
Accepted 10 March 2010

Keywords:
Biodegradation
Cement paste (D)
Durability (C)
Modeling (E)
Organic acids (D)

ABSTRACT

Reactive transport models can be used to assess the long-term performance of cement-based materials subjected to biodegradation. A bioleaching test (with *Aspergillus niger* fungi) applied to ordinary Portland cement pastes during 15 months is modeled with HYTEC. Modeling indicates that the biogenic organic acids (acetic, butyric, lactic and oxalic) strongly accelerate hydrate dissolution by acidic hydrolysis whilst their complexation of aluminum has an effect on the secondary gel stability only. The deepest degradation front corresponds to portlandite dissolution and decalcification of calcium silicate hydrates. A complex pattern of sulfate phases dissolution and precipitation takes place in an intermediate zone. The outermost degraded zone consists of alumina and silica gels. The modeling accurateness of calcium leaching, pH evolution and degradation thickness is consistently enhanced whilst considering increase of diffusivity in the degraded zones. Precipitation of calcium oxalate is predicted by modeling but was hindered in the bioleaching reactor.

1. Introduction

Concrete and cement-based materials operate in chemically aggressive conditions that may damage cement microstructures and limit the material service life. The activities of microorganisms can generate such aggressive aqueous solutions in several specific environments. The main mechanisms of biodegradation usually relate to hydrate alteration and mineralogical transformation by ion exchange between acidic effluents and the cement-based material. Bacteria catalyze the generation of sulfuric acid by hydrogen sulfide oxidation in sewage disposals, which strongly impacts the durability of concrete sewer pipes (e.g. [1,2]). Bacteria and fungi metabolisms produce biogenic carboxylic acids in agro-industrial environments (silage effluents, liquid manure), which can severely damage concrete floors and storage structures (e.g. [3,4]).

A case study of the detrimental impact of microorganisms on ordinary Portland cement matrices has been previously investigated by means of a bioleaching test with the fungus *Aspergillus niger* [5]. Fungi are liable to colonize cement matrices and lead to either a direct (physical) attack by the biofilm coating the material, which results in hyphae penetrating through the accessible pores, and/or to an indirect (chemical) attack by their metabolites [6]: chemical attack is predominant [7,8]. The major organic acids secreted by the fungal culture during the studied bioleaching test consisted of acetic, butyric, lactic and oxalic acids. Cement pastes experienced a substantial leaching of calcium and a significant mechanical degradation highlighted by the drastic decline in Young's modulus.

The complexities arising from having many dissolved and mineral species as well as coupling with advection and diffusion mechanisms are now readily handled by reactive transport codes. These numerical tools can be used to investigate degradation processes at the laboratory scale (leaching tests) as well as to assess of the long-term behavior of similar materials at field scales in view of performance and service life modeling. Many studies have already dealt with the modeling of decalcification of cement-based materials in leaching tests by pure water [9–14] or ammonium nitrate solutions [15]. Complex relationships between microstructural changes and effective diffusivity have been developed in some models [11,12,14]. However, to our knowledge, reactive transport modeling has never been applied for examining the generic case of biogenic acid degradation of cement matrices. Small organic acids have been reported to be important in the weathering of soil due to their ability to complex aluminum [16]. An important question is, therefore, to determine whether microorganism attack is a special case of acid attack on concrete [17], or whether complexation by the conjugated bases is effective too. Another question is the protective effect of organic salt (mainly calcium oxalate) precipitation at the cement surface against biodegradation [4,18].

Thermodynamic data to permit the calculation of interaction between commonly-found organic acids (acetic, butyric, oxalic) and hydrated phases as well as ions in the pore solution of cement at 25 °C are readily available. This paper aims at modeling the fungal bioleaching test [5] with the HYTEC reactive transport model [19] by taking into account: i) the production of organic acids by microorganisms, ii) the chemical mechanisms occurring both in the cement pore water and the bioleaching reactor, iii) the mineralogical alteration of the cement

* Corresponding author. Tel.: +33 1 64 69 49 42; fax: +33 1 64 69 47 13.
E-mail address: laurent.dewindt@mines-paristech.fr (L. De Windt).

0008-8846/$ – see front matter © 2010 Elsevier Ltd. All rights reserved.
doi:10.1016/j.cemconres.2010.03.005

Table 1
Composition of the fungal culture medium; the components considered in the calculations are in bold.

Components	mg/L	Components	µg/L
KH_2PO_4	136	$CuSO_4 \cdot 5H_2O$	0.5
Na_2HPO_4	60	BH_3O_3	1
$MgSO_4 \cdot 7H_2O$	70	$MnSO_4 \cdot H_2O$	1
NH_4NO_3	100	$ZnSO_4 \cdot 7H_2O$	1
$CaCl_2$	10	$Mo_7(NH_4)_6O_{24} \cdot 4H_2O$	10
$FeSO_4 \cdot 7H_2O$	0.2	$Co(NO_3)_2 \cdot 6H_2O$	1
Glucose	10000		

matrix, and iv) the coupled evolution of porosity and diffusivity. The chemical effects (acidity, complexation, salt precipitation) of the biogenic organic acids are analyzed in details, and the model capacity for simulating the extent of cement degradation is estimated with a view to further applications of material performance with respect to biodegradation.

2. Bioleaching test

2.1. Microorganism and culture medium

The acidophilic fungus *A. niger* is ubiquitous and commonly found in soil environments. It is known to colonize mortar [20], and is consequently a suitable candidate for assessing the durability of cement materials with respect to bioleaching phenomena. The composition of the fungal growth medium used in this study is given in Table 1. The fungal culture medium provided the essential nutritional elements needed by the microorganisms for growth and, due to the phosphates, buffered the lixiviating solution in contact with the cement paste in order to prevent alkaline pH. Glucose was supplied as a carbon source (substrate), in order to ensure optimum favorable conditions for fungal growth.

2.2. Cement pastes

The bioleaching test was conducted on pastes made with a Portland cement (CEM-I 52.5 N CP2) whose chemical composition is given in Table 2. The water/cement mass ratio of the pastes was 0.5. The hardened cement paste specimens were cylindrical in form, 220 mm high and 110 mm in diameter. The specimens were demolded 24 h after casting and stored at 20 °C for 27 days in a basic solution (NaOH = 3 g/L, KOH = 10 g/L, corresponding to a pH of 13.6) in order to limit all preliminary leaching of portlandite. A 23% porosity of the cement paste at 28 days was determined by mercury intrusion porosimetry after drying at 50 °C until constant mass.

2.3. Bioleaching protocol

The followed bioleaching procedure provided an accelerated simulation of fungal attack on cement pastes. A set of 12 cement paste specimens were put in contact with the microbial growth medium and *A. niger* in a bioleaching reactor at 20 °C. The test was performed under aerobic condition in order to enhance fungal growth. The L/S mass ratio – mass of the leaching solution divided by the exchange surface of the solid – was 10 g/cm^2. Every 2 weeks, 20% of the leaching (reactor) solution was renewed. *A. niger inoculum* was added regularly to the leaching solution at the same frequency. Two cement paste samples were extracted every 12 weeks for analysis and an adjustment of the leaching solution was done to maintain a constant L/S ratio over time. A control leaching test was also performed in parallel with demineralized water for the sake of comparison.

Table 2
Chemical composition and mineralogy of the hydrated ordinary Portland cement (w/c = 0.5) considered in the calculations.

Oxide	Experiment	Modeling	Mineralogy	Modeling
Al_2O_3	2.9 [wt.%]	2.8 [wt.%]	C–S–H 1.8	49 [wt.%]
CaO	43.3	46.4	Ettringite	9.5
MgO	0.4	0.3	Hydrogarnet	2
SiO_2	14.7	15.5	Hydrotalcite	1.5
SO_3	1.7	2	Portlandite	22
Others	4	–	(Pore water)	16
Water	33	33		

K_2O and Na_2O are 0.05 and 0.025 wt.%, respectively (both for experiment and modeling).

The analyses carried out on the leaching solution included the measurement of electrical conductivity, pH, calcium (by inductively coupled plasma), and biogenic organic acids (by high performance liquid chromatography). The degradation of the cement matrix was examined by scanning electron microscopy (SEM) combined with energy dispersive X-ray (EDX) analysis of polished section. The instrument used was a FEI QUANTA 200 equipped with an Oxford Inca Energy Dispersive X-ray system for chemical analysis of cement paste samples extracted every 12 weeks. Changes in elements along three transverse lines on the specimen surface were carried out. Analyses were performed under a tension of 15 kV in empty low mode. The depth of interaction depends on the density of elements. The optimal resolution (129 eV) was determined on manganese. The pear of interaction was 2 µm^3.

3. Modeling approach and data

3.1. Reactive transport modeling

To describe the evolution of the mineral phases in time and in space requires the coupling of chemistry with hydrodynamic migration processes. HYTEC has been developed for the purpose of solving migration and chemical processes and can be used for calculating profiles as a function of time, type of attack solution and cement composition [19]. HYTEC is based on a finite volume scheme with representative (homogenized) elementary volumes (REV) for mass transport and a sequential iterative operator-splitting method for coupling between chemistry and transport. Diffusion is the main transport mechanism considered in the present study. This mass transport process is coupled to chemistry according to the following equation under water-saturated conditions (as for the present bioleaching protocol):

$$\frac{\partial \omega c_i}{\partial t} = \nabla \cdot (D_e \nabla c_i) - \frac{\partial \omega \bar{c}_i}{\partial t}, \quad (1)$$

where the term D_e is the effective diffusion coefficient, ω is the porosity, c_i and $\bar{c}_i$ are the mobile and immobile concentrations of element per unit volume of solution, respectively. The fixed or solid fraction is evaluated by the chemical calculations, whilst the aqueous fraction is a function of diffusion only.

The porosity is explicitly included in Eq. (1) since this entity is subjected to change in time and space when mineral precipitation or dissolution modifies the local porosity. Thus, HYTEC accounts for pore clogging by carbonation, or on the contrary, for porosity increase by leaching of hydrates. The change in specific volume of the cement phases can be calculated by HYTEC from the evolution of the mineral concentrations in the system, knowing their density. Several porosity–diffusion relations are found in the literature, some being specific to cements and concretes. The empirical Archie's law is easy to implement in reactive transport models and applicable to a wide range of materials. A modified version of Archie's law was consequently used in a first attempt at modeling the feedback of chemistry on mass transport:

$$D_e(\omega) = D_e(\omega_0)\left(\frac{\omega - \omega_c}{\omega_0 - \omega_c}\right)^m, \quad (2)$$

where ω_0 is the initial porosity, ω_c is a critical porosity threshold under which diffusion stops and m is an empirical Archie's coefficient.

More complex and precise relationships to predict the macroscopic diffusivity can be developed. For example, homogenization models allow to obtain macroscopic diffusion coefficients of cementitious materials taking into account the microscopic properties [12,14]. These models are more complex to include in reactive transport models since they need information about microscopic geometries of matrix-forming minerals. Archie's law provides a simple approach to reproduce the expected tendencies of Portland cement leaching. A zero porosity threshold and an Archie's coefficient of 4 were used in this study, as discussed in Section 4.3.

3.2. Configuration and hydrodynamic data

The configuration of the bioleaching reactor was simplified to a one-dimensional section (parallelepiped nodes) including the cement paste and the bioleaching reactor. The node size of the calculation grid was set to 0.2 mm. This simplified configuration complied with the experimental L/S (10 g/m^2) and the renewal rate of the bioleaching solution.

In the model, the initial porosity, ω_0, of the cement pastes was rounded up to 25% and the effective diffusion coefficient, $D_e(\omega_0)$, was set to 3×10^{-12} m^2/s. HYTEC only takes into account a common coefficient for both cationic, neutral and anionic species. These porosity and effective diffusion coefficient values are close to data published on similar CEM-I paste (w/c ~ 0.5, [11,12]). Temperature was fixed to 20 °C in both the cement paste and the bioleaching reactor zones of the calculation grid.

3.3. Thermodynamic data and initial mineralogy

The chemical reactions were calculated assuming thermodynamic equilibrium, i.e. chemical reactions are assumed to be instantaneous compared to diffusion, and using the B-dot activity model for ionic strength correction. One essential step of the modeling was to select relevant data for the acid/base and complexation properties of the main organic acids (acetic, butyric, lactic, oxalic). The MINTEQ thermodynamic database [21] – release 2.20 – was selected due to its dataset of organic acids. This database includes most of the relevant thermodynamic constants but a few ones were taken from the HATCHES database [22]. Tables 3 and 4 detail the equilibrium formation constants of the Al–Ca–Mg organometallic and hydroxyl complexes used in the present calculations. These formation constants are very close to the values selected independently for discussing the effects of organic acids on the dissolution of silicate minerals [23]. Data on lactic complexes were lacking in both the MINTEQ and HATCHES databases.

The MINTEQ database was also enriched with additional thermodynamic constants for cement-type minerals, as reported in Table 5. The decalcification of calcium and silicate hydrate (C–S–H), which implies a progressive decrease of their Ca/Si ratio during degradation. A discrete approach of C–S–H dissolution was used by considering C–S–H 1.8, C–S–H 1.1 and C–S–H 0.8. Aluminum hydroxide (gibbsite) and silica gel (amorphous SiO_2) were considered as ultimate degradation stages. AFm (calcium monosulfo-aluminate), AFt (ettringite), CH (portlandite) and C_3AH_6 (hydrogarnet) and hydrotalcite were also introduced in the database. Acetate and butyrate salts of calcium are known to be soluble [4]. By contrast, calcium oxalate solubility is low [29] and this mineral was included in the database. Data on aluminum oxalate were lacking in both the MINTEQ and HATCHES database.

The mineralogy of the hydrated cement paste considered in the modeling was based on the measured chemical composition and XRD

Table 3
Equilibrium constants of reactions (mass balance equations) corresponding to the formation of the Al–Ca–Mg organic complexes considered in the calculations.

Species	Reaction	Log*K* (25 °C)	Ref.
H-acetate	$H^+ + C_2H_3O_2^- \rightarrow C_2H_4O_2$ ($C_2H_4O_2 = CH_3–COOH$)	4.8	[21]
Al-acetate^{2+}	$Al^{3+} + C_2H_3O_2^- \rightarrow AlC_2H_3O_2^{2+}$	2.6	[21]
Al-(acetate)$_2^+$	$Al^{3+} + 2C_2H_3O_2^- \rightarrow Al(C_2H_3O_2)_2^+$	4.3	[21]
AlOH-acetate$^+$	$Al^{3+} + C_2H_3O_2^- + H_2O \rightarrow AlOHC_2H_3O_2^+ + H^+$	−0.2	[21]
$Al_2(OH)_2$-acetate^{3+}	$2Al^{3+} + C_2H_3O_2^- + 2H_2O \rightarrow Al_2(OH)_2C_2H_3O_2^{3+} + 2H^+$	−2.4	[21]
Ca-acetate$^+$	$Ca^{2+} + C_2H_3O_2^- \rightarrow CaC_2H_3O_2^+$	1.2	[21]
Ca-(acetate)$_2$	$Ca^{2+} + 2C_2H_3O_2^- \rightarrow Ca(C_2H_3O_2)_2$	4.0	[22]
Mg-acetate$^+$	$Mg^{2+} + C_2H_3O_2^- \rightarrow MgC_2H_3O_2^+$	1.3	[21]
H-butyrate	$H^+ + C_4H_7O_2^- \rightarrow C_4H_8O_2$ ($C_4H_8O_2 = CH_3CH_2CH_2–COOH$)	4.8	[21]
Al-butyrate^{2+}	$Al^{3+} + C_4H_7O_2^- \rightarrow AlC_4H_7O_2^{2+}$	2.2	[21]
Ca-butyrate$^+$	$Ca^{2+} + C_4H_7O_2^- \rightarrow CaC_4H_7O_2^+$	0.9	[21]
Mg-butyrate$^+$	$Mg^{2+} + C_4H_7O_2^- \rightarrow MgC_4H_7O_2^+$	1.0	[21]
H_2-oxalate	$2H^+ + C_2O_4^{2-} \rightarrow C_2H_2O_4$ ($C_2H_2O_4 = HOOC–COOH$)	5.4[a]	[21]
H-oxalate$^-$	$H^+ + C_2O_4^{2-} \rightarrow C_2HO_4^-$	4.2	[21]
Al-oxalate$^+$	$Al^{3+} + C_2O_4^{2-} \rightarrow AlC_2O_4^+$	7.7	[21]
Al-(oxalate)$_2^-$	$Al^{3+} + 2C_2O_4^{2-} \rightarrow Al(C_2O_4)_2^-$	13.4	[21]
Al-(oxalate)$_3^{3-}$	$Al^{3+} + 3C_2O_4^{2-} \rightarrow Al(C_2O_4)_3^{3-}$	17.0	[21]
Al-Hoxalate^{2+}	$Al^{3+} + C_2O_4^{2-} \rightarrow AlC_2HO_4^{2+}$	7.5	[21]
AlOH-oxalate	$Al^{3+} + C_2O_4^{2-} + H_2O \rightarrow AlOHC_2O_4 + H^+$	2.6	[21]
AlOH-(oxalate)$_2^{2-}$	$Al^{3+} + 2C_2O_4^{2-} + H_2O \rightarrow AlOH(C_2O_4)_2^{2-} + H^+$	6.8	[21]
Al(OH)$_2$-oxalate$^-$	$Al^{3+} + C_2O_4^{2-} + 2H_2O \rightarrow Al(OH)_2C_2O_4^- + 2H^+$	−3.1	[21]
Ca-oxalate	$Ca^{2+} + C_2O_4^{2-} \rightarrow CaC_2O_4$	3.2	[21]
Ca-(oxalate)$_2^{2-}$	$Ca^{2+} + 2C_2O_4^{2-} \rightarrow Ca(C_2O_4)_2^{2-}$	8.1	[22]
Mg-oxalate	$Mg^{2+} + C_2O_4^{2-} \rightarrow MgC_2O_4$	3.6	[21]
Mg-(oxalate)$_2^{2-}$	$Mg^{2+} + 2C_2O_4^{2-} \rightarrow Mg(C_2O_4)_2^{2-}$	5.1	[22]

[a] Corresponding to $pK_{a1} = 1.2$ and $pK_{a2} = 4.2$ for the oxalic dicarboxylic acid.

Table 4
Equilibrium constants of reactions (mass balance equations) corresponding to the formation of the Al–Ca–Mg-hydroxyl complexes considered in the calculations.

Species	Reaction	Log*K* (25 °C)	Ref.
Al-hydroxyl^{2+}	$Al^{3+} + OH^- \rightarrow AlOH^{2+}$	9.0[a]	[21]
Al-(hydroxyl)$_2^+$	$Al^{3+} + 2OH^- \rightarrow Al(OH)_2^+$	17.7	[21]
Al-(hydroxyl)$_3$	$Al^{3+} + 3OH^- \rightarrow Al(OH)_3$	25.3	[21]
Al-(hydroxyl)$_4^-$	$Al^{3+} + 4OH^- \rightarrow Al(OH)_4^-$	33.3	[21]
Ca-hydroxyl$^+$	$Ca^{2+} + OH^- \rightarrow CaOH^+$	1.3	[21]
Mg-hydroxyl$^+$	$Mg^{2+} + OH^- \rightarrow MgOH^+$	2.2	[21]

[a] The formation constants are given in terms of OH^- to allow for a direct comparison with the organic complex data of Table 3.

Table 5
Equilibrium constants of reactions (mass balance equations) corresponding to the formation of the solid phases and volumic weights considered in the calculations.

Mineral	Reaction	Log*K* (25 °C)	Density (kg/m^3)	Ref.
Calcite	$Ca^{2+} + CO_3^{2-} \rightarrow CaCO_3$	8.5	2.7×10^3	[21]
Ca-Oxalate	$Ca^{2+} + C_2O_4^{2-} \rightarrow Ca\text{-}C_2O_4{:}H_2O$	8.8	2.2×10^3	[21]
C–S–H 0.8	$0.8Ca^{2+} + H_4SiO_4 - 0.4H_2O \rightarrow$ C–S–H $0.8 + 1.6H^+$	−11.1	2.2×10^3	[24[a]]
C–S–H 1.1	$1.1Ca^{2+} + H_4SiO_4 + 0.2H_2O \rightarrow$ C–S–H $1.1 + 2.2H^+$	−16.7	2.2×10^3	[24[a]]
C–S–H 1.8	$1.8Ca^{2+} + H_4SiO_4 + 1.6H_2O \rightarrow$ C–S–H $1.8 + 3.6H^+$	−32.6	2.2×10^3	[24[a]]
Ettringite	$2Al^{3+} + 6Ca^{2+} + 3SO_4^{2-} + 38H_2O \rightarrow Ca_6Al_2(SO_4)_3(OH)_{12}{:}26H_2O + 12H^+$	−56.9	1.8×10^3	[25]
Gibbsite	$Al^{3+} + 3H_2O \rightarrow Al(OH)_3 + 3H^+$	−8.8	2.4×10^3	[21]
Gypsum	$Ca^{2+} + SO_4^{2-} + 2H_2O \rightarrow CaSO_4{:}2H_2O$	4.9	2.3×10^3	[21]
Hydrogarnet	$2Al^{3+} + 3Ca^{2+} + 6H_2O \rightarrow Ca_3Al_2(OH)_{12} + 12H^+$	−78.9	3.0×10^3	[26[b]]
Hydrotalcite	$2Al^{3+} + 4Mg^{2+} + 10H_2O \rightarrow Mg_4Al_2O_4(OH)_6 + 14H^+$	−73.8	2.1×10^3	[27]
Monosulfo-aluminate	$2Al^{3+} + 4Ca^{2+} + SO_4^{2-} + 12H_2O \rightarrow Ca_4Al_2SO_4(OH)_{12} + 12H^+$	−73.0	1.9×10^3	[28]
Portlandite	$Ca^{2+} + 2H_2O \rightarrow Ca(OH)_2 + 2H^+$	−22.7	2.2×10^3	[21]
Silica gel	$H_4SiO_4 \rightarrow SiO_2 + 2H_2O$	2.8	2.1×10^3	[21]

[a] The constant was fitted on the experimental data.
[b] Constant of katoite.

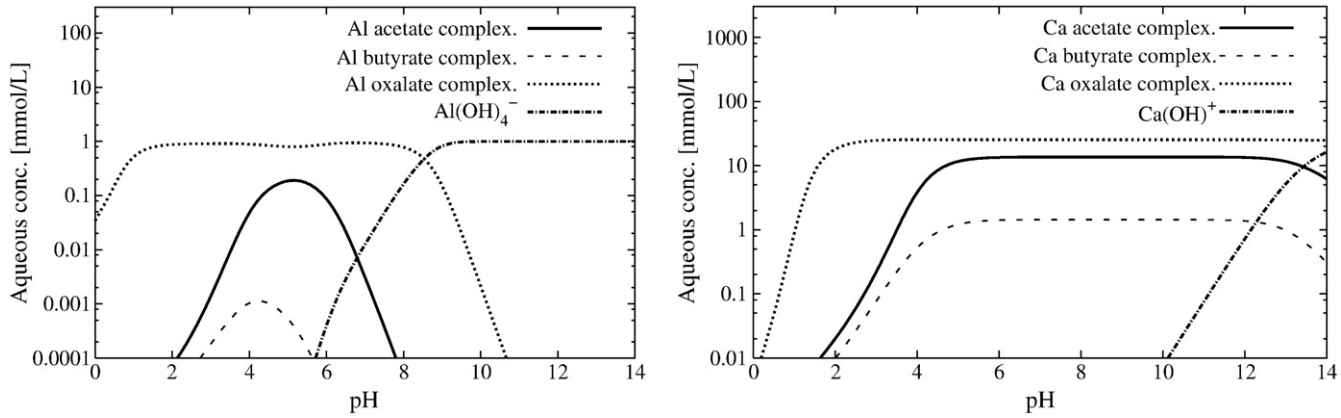

Fig. 1. Calculated pH dependency of aluminum and calcium complexation by organic acids at 25 °C; the metal and organic acid concentrations are representative of the bioleaching test.

analysis (Table 2): C–S–H 1.8 (55% by weight content), portlandite (25%), ettringite (11%), hydrogarnet (2.5%) and hydrotalcite (2%). The calculated pore water chemistry was typical of a Portland cement with a pH above 13.

4. Modeling results and discussion

4.1. Organic acid chemistry

The major organic acids secreted by the fungal culture during the bioleaching test consisted of 4 carboxylic acids: acetic, butyric, lactic and oxalic acids. Acetic ($pK_a = 4.75$), butyric ($pK_a = 4.80$), lactic ($pK_a = 3.9$) and oxalic ($pK_{a1} = 1.2$, $pK_{a2} = 4.2$) acids are all weak acids though the first oxalic acid function is relatively strong.

In aqueous solution, Al^{3+} and Ca^{2+} cations are complexed by the conjugated bases of the organic acids (i.e. acetate, butyrate and oxalate anions). Fig. 1 reports the pH dependency of aluminum and calcium complexation calculated with HYTEC for concentrations representative of the present bioleaching test. Aluminum complexation by organic acid ligands is predominant in the pH range 0 to 10, but the hydroxyl complex $Al(OH)_4^-$ is the most stable species at alkaline pH. This means that the presence of organic acids should not significantly modify aluminum chemistry in the pore water of the cement paste. Their effect should become dominant when pH drops below 10 in the degraded cement zones. Wang et al. [16] experimentally showed that acetate complexation did not significantly modify gibbsite precipitation, but that oxalate interacted more strongly with aluminum and increased the aluminum hydroxide solubility between pH 4 and 9. By contrast, complexation of calcium by organic acid ligands is effective in the full pH range since the hydroxyl complex $Ca(OH)^+$ is relatively weak. At equivalent concentrations, oxalate has the greatest affinity for both aluminum and calcium whereas butyrate presents the weakest affinity. The range of acidity constants (pK_a) also implies that oxalate complexes are formed at lower pH ($pH \geq 2$) than acetate and butyrate ones ($pH \geq 5$).

Fig. 2 presents solubility diagrams for aluminum and calcium calculated with HYTEC in pure water and in oxalic acid solutions, at concentrations representative of the bioleaching test. Gibbsite was used as a substitute for the alumina gel formed during bioalteration (Section 4.4). Gibbsite solubility is particularly low in the pH range 5–9, which promotes alumina gel formation in degraded cement layers. Ettringite dissolution is the main aluminum source in the present case. By comparison, the apparent gibbsite solubility is clearly enhanced in the presence of oxalic acids at acidic and neutral pH, but not at alkaline pH. The behavior of calcium is significantly different. Strongly soluble (at least in the absence of carbonates or sulfates), calcium becomes relatively insoluble in the presence of oxalic acids. The higher the oxalate concentration, the more efficient is complexation, and the higher the apparent calcium solubility.

4.2. Evolution of chemistry in the bioleaching reactor

Fig. 3 shows the evolution over time of the concentration of the main biogenic organic acids produced by the fungal culture. Minor contents in citric, formic, gluconic and propionic acids were analyzed. However, the predominant organic acids were acetic, butyric, lactic and oxalic acids during all the duration of the bioleaching test. The temporal evolution of the biogenic acid concentrations was typical of microbial activity in a batch culture media, with a preliminary exponential growth followed by a stationary regime whereby production and destruction of organic acids are counterbalanced. During the transitional regime, the total quantity of organic acids progressively increased to level off between 300 and 400 mmol/L. This concentration level is high but comparable to the concentration of organic acids in aggressive agricultural environments (silage, slurry etc.).

The fluctuations of organic acid concentration were partly due to the difficulty of maintaining a constant input of glucose during all the experiment. The concentrations of oxalic and butyric acids were relatively constant (Fig. 3). The proportion of lactic acids was below 10% of total acids for the first 8 months and then increased to reach 30% of total acids. In parallel, acetic acids followed an inverse trend compared with lactic acids. This phenomenon could be explained by a change in the metabolism of the microorganisms present in the lixiviating solution as from the 8th month which favored the production of lactic acid to the detriment of acetic acid. The detailed modeling of the microbial activity is very complex and is far beyond the objectives of this paper. The production rate of the various organic acids was fitted on the measured experimental data considering average stationary concentrations without fluctuation. The well balanced inversion at 8 months between acetic and lactic acid concentrations was not introduced in the model due to the lack of data on lactate complexes. Acetic acid was assumed to be a reasonable substitute for lactic acid in the present study.

The dissolved calcium concentration and pH in the bioleaching reactor are also reported in Fig. 3. Their evolutions over time closely followed the production curve of the biogenic organic acids, which indicates that cement bioleaching actually corresponds to a chemical attack by organic acids. The stationary pH within the bioleaching reactor was weakly acidic, varying between 4 and 5, with occasional increases in pH probably due to a lack of glucose in the fungal growth medium. When there is a shortage of glucose, the organic acids produced by the fungi may, in their turn, be assimilated and degraded, which could explain these increases in pH. The pH of the bioleaching reactor was significantly lower than the pH of the control test, which was around 12. In parallel, the concentration of dissolved calcium also

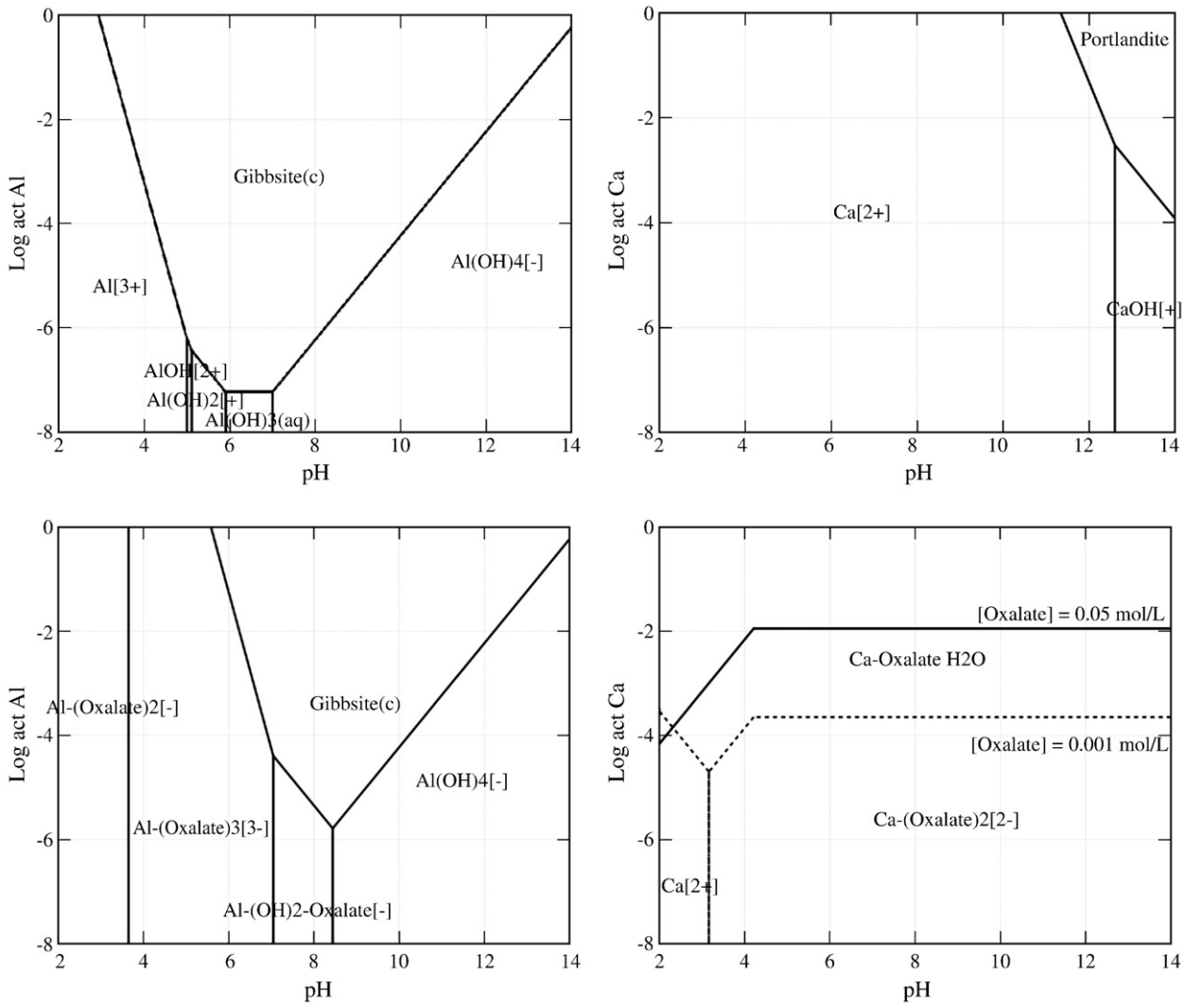

Fig. 2. Calculated solubility diagrams for aluminum and calcium in pure water (top graphs) and with dissolved oxalic acids (bottom graphs) at 25 °C; oxalic acid concentrations are set to 0.001 mol/L for aluminum, 0.001 mol/L and 0.05 mol/L for calcium.

showed an increasing trend and reaches a value of 100 mmol/L. The total amount of leached calcium was high compared to the control test; i.e. 20 times higher in average, as shown in Fig. 3.

The modeling results are in good agreement with the experimental data. In particular, the model correctly reproduces the strong contrast in leached calcium and pH between the bioleaching test and the control test. For both pH and leached calcium, the stationary plateau is due to the balance between leaching and renewal of the solution. The model failed to simulate the early pH trend and would have required a better description of the early production of organic acids. The calculated initial pH value of the $H_2PO_4^-$–HPO_4^{2-} buffer (pH<8) is correct. Nevertheless, the buffering capacity is not efficient enough to neutralize the alkaline peak at the early stage (notably, the fast lixiviation of K^+ and Na^+ alkalis) in the calculations. Furthermore, the calculated pH is systematically lower than the bioleaching data by one pH unit. Obviously, the complexity of the microorganism activities cannot be reduced to the single production of four biogenic acids though this simplification works reasonably well in the present modeling study.

4.3. Degradation depths

The concentration gradient between the reactor solution and the cement pore water provokes ionic diffusion, in particular the biogenic organic acids readily diffuse into the cement pores bringing about hydrate dissolution. The measured thickness of the degraded zone (i.e. characterized by hydrate leaching compared to the initial mineralogy of the cement paste) after 15 months of bioleaching was about 8–9 mm. The thickness of the degraded zone was 5 times larger than the degradation thickness found in the control test (1.5 mm). Experimentally, the thicknesses of the degraded zone were determined by optical microscopy and distribution of oxides along a transverse (Section 4.5). It is worth noting that hyphae of the fungi were not observed to penetrate the cement paste surface [5]. Hence, cement alteration was driven by chemical attack and not by physical disruption.

The agreement between the calculated and experimental depths was strongly dependent on the law that couples mineralogical evolution, porosity and diffusion. The consistency, and interdependency, between the calculated degraded thickness and the calculated pH of the bioleaching reactor is worth noting. The better the degraded thickness, the better the pH value is. As shown in Fig. 4, a fixed porosity approach obviously underestimates the degradation depth. The degradation of cement and concrete is controlled by the effective diffusion coefficient. The smaller the coefficient, the lower the exchange of dissolved ions with the leaching solution and the slower the degradation. It is thus essential to correctly estimate the initial diffusion coefficient but, in addition, to consider the enhancement of the diffusion process in the degraded zones. The application of Archie's

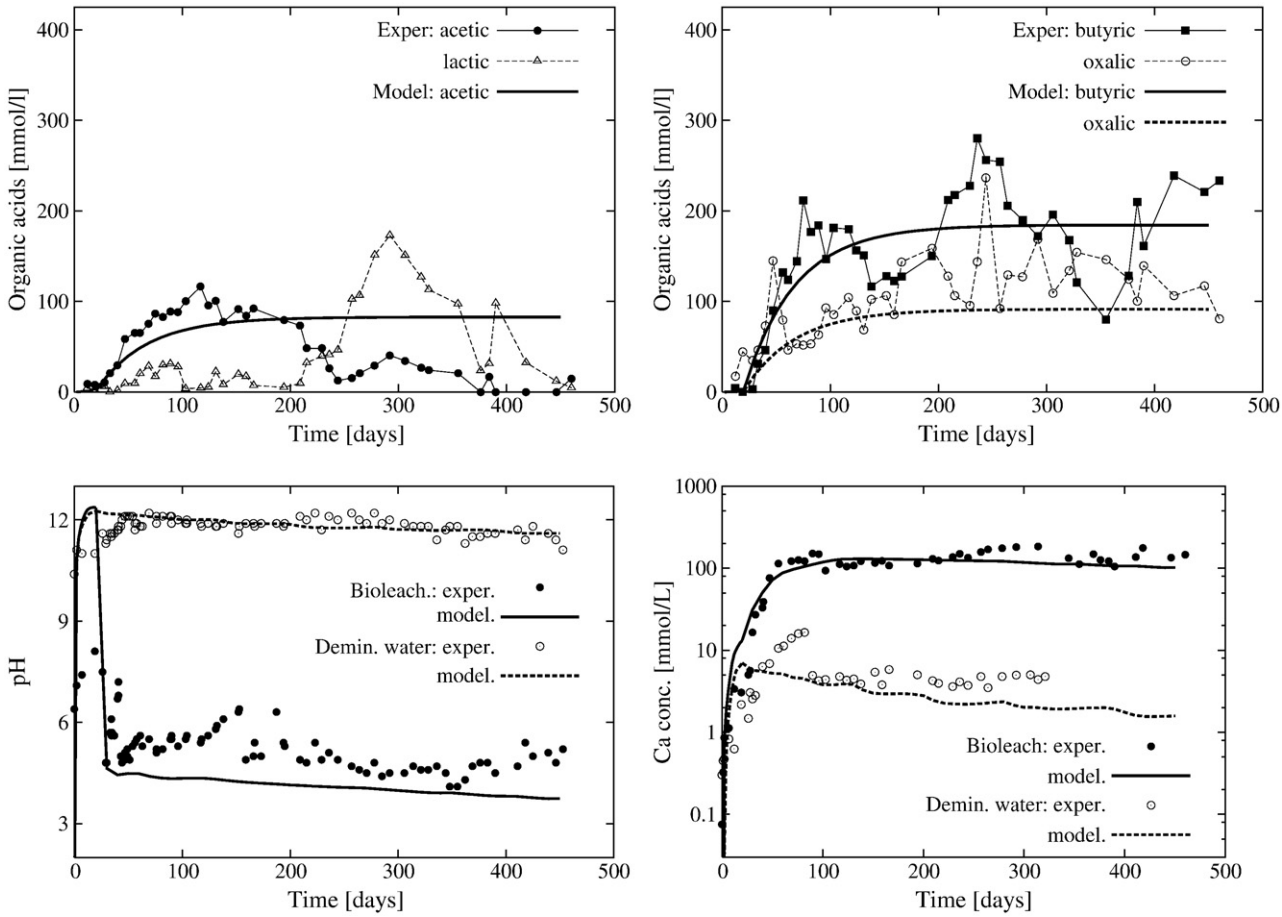

Fig. 3. Top: experimental and fitted evolution over time of the dissolved organic acids; bottom: experimental and calculated evolutions over time of the reactor chemistry (pH and dissolved calcium), comparing the bioleaching test and the control test (demineralized water).

relationship increased the quality of the modeling (Fig. 4). An Archie's coefficient between 2 and 3 and a zero porosity threshold have been commonly used for modeling the degradation of cement-based materials [30,31]. However, the degradation stage was so advanced in the present case that an Archie's power of 4 better matched the very open porous gel structure found in the most degraded zone of the cement matrix.

The degraded layer had almost no protective effect (diffusive barrier) in the present experiment, both experimentally and by calculation, as indicated by the almost linear increase of degradation depths with time in Fig. 4. Highly porous cored layers consisting mainly of silica gel have been mentioned in literature [17,32]. The leaching process was shown to produce an extreme coarsening of the pore size distribution and to a large increase in porosity, boosting the transport of ions in the degraded layer. In these experimental studies, effective diffusion coefficient of degraded cement and mortar was more than one order of magnitude larger than the values of the non degraded material. In the present

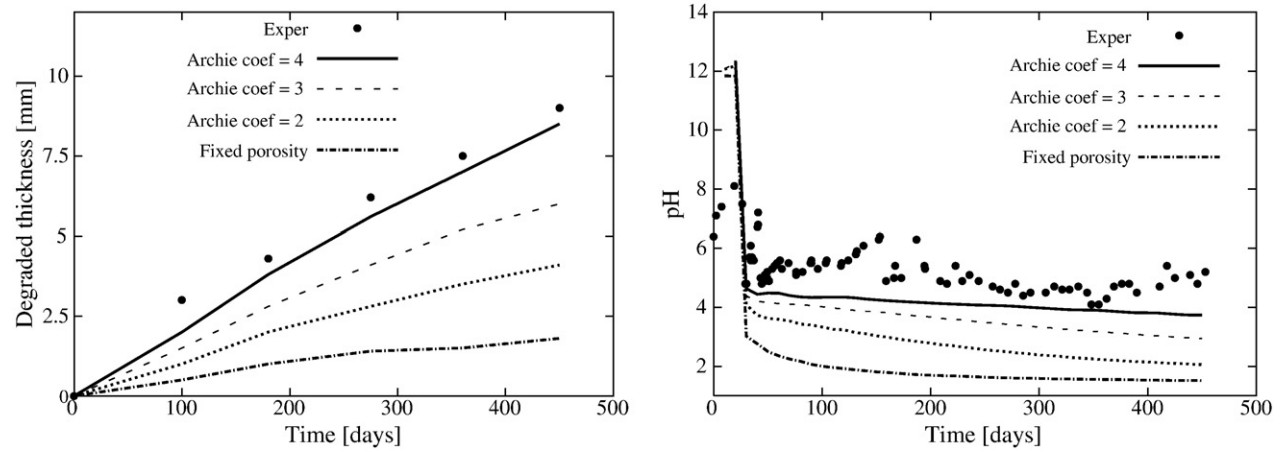

Fig. 4. Effect of the Archie's coefficient m (Eq. (2)) on the calculated biodegradation thickness inside the cement paste (left) and on the calculated pH in the bioleaching reactor (right) for coupled chemistry/diffusion calculations; a fixed porosity approach corresponds to a zero Archie's coefficient.

study, the calculated effective diffusion coefficient of the most degraded layer ($D_e \sim 1.5 \times 10^{-10}$ m^2/s) was 50 times higher compared to the initial value. The calculated porosity increases from 25% in the sound zone to approximately 65% in the most degraded layer. This agrees relatively well with the experimental values: the porosity of the sound zone and the most degraded zone were 23% and 56%, respectively.

4.4. Modeling of the mineralogy of the degraded zones

Fig. 5 shows the mineralogical profiles calculated along a transverse after 450 days of bioleaching. Three distinct zones can be identified from the sound zone to the edge of the cement paste: i) the sound zone itself, ii) an intermediate less degraded zone, distinguished by a dense structure [5], and iii) an outermost strongly degraded zone, characterized by a much open porosity [5].

4.4.1. Intermediate degraded zone

The deepest degradation front corresponds to portlandite dissolution and decalcification of the primary calcium silicate hydrate due to reaction with the organic acids. For instance, in the case of acetic acid, the chemical equations globally write as follows:

$$CH + 2H - acetate \rightarrow Ca - (acetate)_2 + 2H_2O \quad (3)$$

$$C\text{–}S\text{–}H1.8 + 3.6H - acetate \rightarrow 1.8Ca - (acetate)_2 + H_4SiO_4 + 1.6H_2O \quad (4)$$

The hydroxyl ions contained in the hydration products are neutralized by the protons of the organic acids. The constitutive ions are consequently dissolved in the pore solution, and then re-precipitate, or diffuse towards the cement paste surface. A complex pattern of sulfate phases dissolution and precipitation also takes place in the intermediate degraded zone. Ettringite dissolution yields gibbsite and gypsum precipitation:

$$AFt + 6H - acetate \rightarrow 3Ca - (acetate)_2 + 2gibbsite + 3gypsum + 26H_2O \quad (5)$$

A significant increase of XRD peaks supported such a re-precipitation of ettringite [5]. The occurrence of the present successive leaching fronts (portlandite, then C–S–H, and eventually ettringite) is a common observation of cement degradation by acid attack [17]. Finally, hydrotalcite is dissolved simultaneously to portlandite. The potential transient re-precipitation of hydrotalcite is most probably a modeling artifact.

Carbon dioxide released during microbial respiration can lead to a complementary carbonic acid attack (or carbonation mechanism):

$$portlandite + H_2CO_3 \rightarrow calcite + 2H_2O \quad (6)$$

Experimentally, XRD patterns indicated a precipitation of calcite in the intermediate degraded zone [5]. Calcite precipitation was also predicted by modeling at the boundary of the sound zone (Fig. 5). The only source of carbon dioxide in the calculation was linked to the renewal solution that was assumed to be in equilibrium with the atmosphere. Obviously, this weak source only yielded small amounts of calcite. In reality, the higher the microbial respiration, the stronger the production of carbon dioxide and the greater the precipitation of calcite. However, the lack of accurate data on microbial respiration in the present study did not allow for a quantitative estimation of biogenic-induced calcite precipitation.

4.4.2. Outermost strongly degraded zone

Both experimentally [5] and in the calculations, the outermost degraded layer was made up of alumina and silica gels. The silica gel was represented in the modeling by the amorphous SiO_2 solid phase. The formation of alumina gel (substituted by gibbsite in the calculations) is induced by the dissolution of ettringite and hydrogarnet, according to Eq. (5). The alumina gel close to the edge is re-dissolved at a later stage in the calculations (Fig. 5) but not in reality, as discussed in the next section. The formation of alumina and silica gels is in agreement with the study of Bertron et al. who have investigated the effect of organic acids on cement pastes in an agricultural context [4,32]. These authors have reported decalcification of the degraded zone, progressive dissolution of all crystallized phases and the possible formation of a silica gel enriched with silicon, aluminum and iron in the superficial layer. According to literature [17], a small amount of calcium remains within the gel layer at pH between 4 and 7 but is completely leached for lower pH. This observation was correctly verified in the present study, both experimentally and by modeling.

4.5. Oxide compositions along a transverse

Fig. 6-graph A shows the measured quantitative oxide compositions along a transverse from the sample edge for a cement paste subjected to bioleaching for 450 days. Despite some noise resulting from the heterogeneity of hydrated cement paste, calcium content gradually

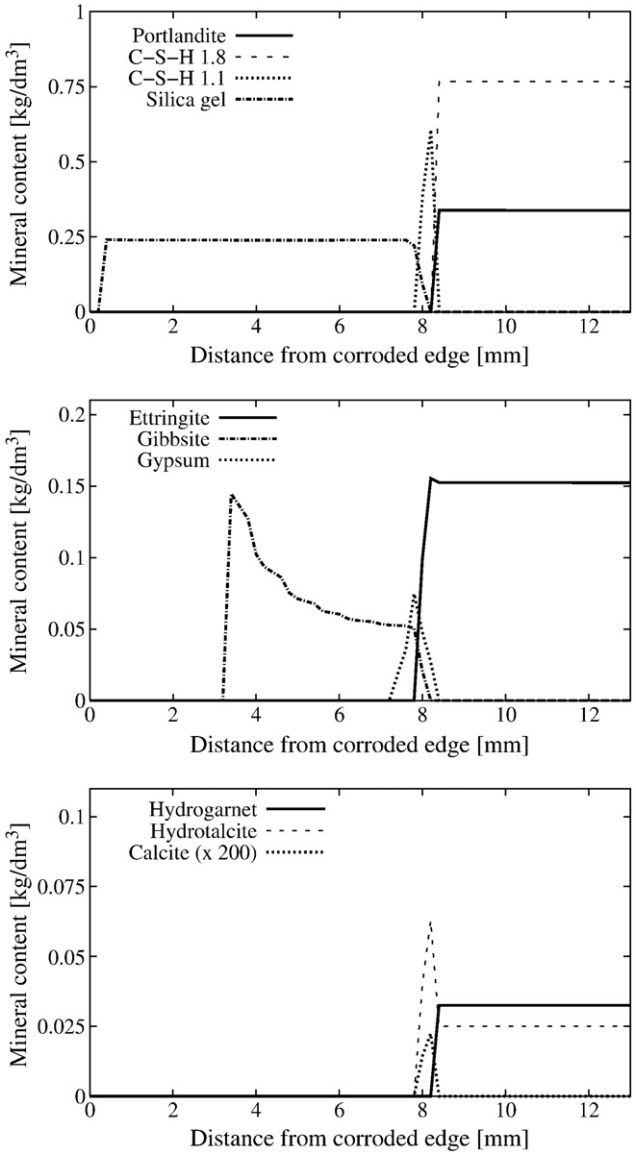

Fig. 5. Calculated mineralogical profiles along a transverse from the edge of the cement paste after 450 days of bioleaching.

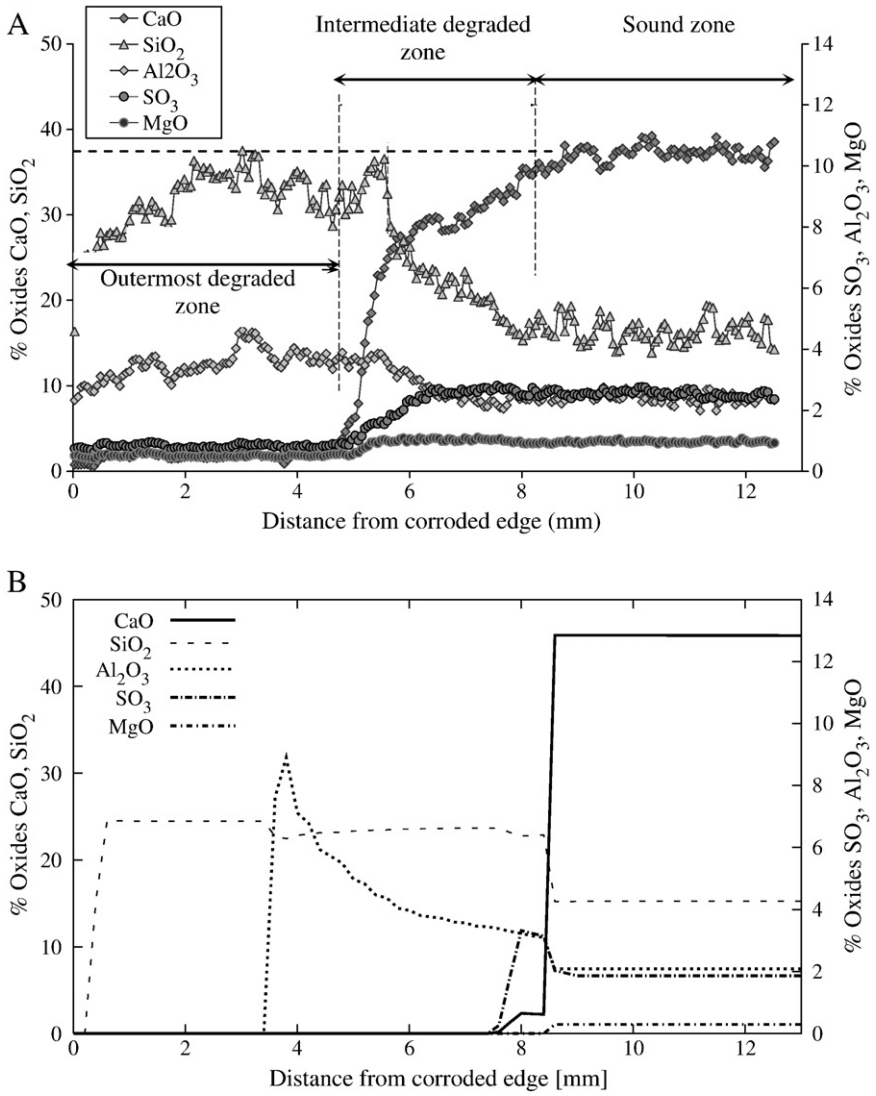

Fig. 6. Experimental (A) and calculated (B) distributions of chemical elements (expressed as oxides) along a transverse from the edge of the cement paste subjected to bioleaching for 450 days.

decreases in the intermediate degraded zone. In the outermost strongly degraded zone, the percentage silicon and aluminum contents significantly increase compared to the sound zone due to the drastic depletion of calcium and sulfate.

Fig. 6-graph B shows the calculated profiles of oxide compositions along the same transverse. The location of the non degraded sound zone is well reproduced as well as the general profile of silicon oxide, which significantly increases in the most degraded zone. A relative enrichment of the intermediate zone in sulfate is calculated similarly to the measured profile. The calculated depletion in magnesium takes place deeper in the cement paste compared to experiment. The silicon oxide content of the most degraded zone was identical to the sound zone in the modeling. A complete depletion of silica occurred both in calculations and experimentally at the outermost zone of the cement paste, over about 0.2 mm.

Though the calculated mineralogical transformations were in agreement with the literature, the model failed to simulate the actual thickness of the intermediate degraded zone, which was about 1 mm in the calculation but 2.5 mm in reality. The combination of representative (homogenized) elementary volumes and thermodynamic equilibrium seems to spatially concentrate the C–S–H decalcification process (Section 4.4) that may be in reality more heterogeneous and/or partly controlled by kinetics. A second major discrepancy between modeling and experiment concerned the width of the aluminum profile in the outermost degraded zone. The precipitation of the aluminum gel, which was substituted by gibbsite in the present modeling, was a sensitive matter in the present calculations. Contrarily to experiment, the aluminum profile is not distributed over the whole degraded layer. As shown in Fig. 6, aluminum is fully leached over the first 3.5 mm of the degraded zone even without considering any aluminum complexation by the organic acids. Moreover, the alumina gel would be totally leached within the intermediate degraded zone, but still present in the intermediate zone, if aluminum complexation was taken into account. This can be interpreted according to the aluminum solubility diagrams of Section 4.1 (Fig. 2): gibbsite precipitation is hindered at pH below 4 in pure water, but as soon as pH drops below 6 in the presence of oxalates. The lack of gibbsite precipitation in the modeling is thus due to the relatively low calculated pH value (pH = 4). In addition, the mixed alumina/silica gel might not be properly modeled by an independent combination of amorphous SiO_2 and gibbsite, as assumed in the present modeling work.

4.6. Remarks on the biogenic organic acid aggressiveness

A complementary calculation was performed without considering aluminum and calcium complexation by acetate, butyrate and oxalate. The degradation depth at 450 days of bioleaching was identical to the one

calculated by considering complexation. This indicates that cement degradation was essentially driven in the modeling by the acidic function of the organic acids (i.e. an acidic hydrolysis) and that complexation had no effect on the degradation depth. This is supported by published experimental works where the formation constants of organometallic complexes (acetic, butyric and lactic acids) had been shown to have no significant effect on the acid attack intensity (decalcification) on Portland cement pastes [4]. On the other hand, as discussed above, aluminum complexation has a significant effect in the modeling on the stability of the alumina gel layer that is formed in the degraded layer, or at least in the proportion of aluminum inserted into the silica gel.

No precipitation of calcium acetic/lactic/butyric salts was observed in the experiments of Bertron et al. mentioned in the previous paragraph [4]. By contrast, recent complementary experiments on cement attack by oxalic acid solutions showed an early precipitation of calcium oxalate salts at the surface of the cement pastes [18]. These oxalate crystals accumulated in the pores of the cement matrix. Such a localized precipitation seemed to have blocked the pores and to act as a barrier against diffusion, thus limiting calcium leaching. In the present bioleaching study, a significant precipitation of calcium oxalate was also calculated by HYTEC at the external boundary of the silica gel in a thermodynamic equilibrium approach. This led to a dramatic decrease of calcium concentration in the reactor in disagreement with the experimental data. Moreover, X-ray diffraction analysis [5] did not indicate any significant formation of calcium oxalates apparently because these crystals were not sufficiently abundant. Only SEM examination of the degrading cement paste specimens pointed out a very few occurrences of calcium oxalate crystals in zone 1 [5]. The reason for the weak calcium oxalate formation is unknown. Consequently, the present modeling did not consider this process in a first approximation.

5. Conclusion

Ordinary Portland cement pastes were severely attacked during bioleaching with an *A. niger* fungal culture, especially by biogenic organic acids (acetic, butyric, lactic and oxalic), and to a lesser extent respiration-induced carbonic acid. Biodegradation was not affected by any physical disruption such as hyphae penetration. The availability of thermodynamic data on organic acids (pK_a, aluminum, calcium, magnesium complexes) has allowed for a coupled chemical and hydrodynamic modeling of this bioleaching test. The production rate of the various organic acids was fitted on the measured experimental data considering average stationary concentrations without fluctuation. The HYTEC model has then been applied to both the bioleaching and control tests. It has been shown that organic acids react with hydrates (portlandite, C–S–H, and ettringite) leading to several degraded zones. The deepest degradation front corresponds to portlandite dissolution and decalcification of calcium silicate hydrates. A complex pattern of sulfate phases dissolution and precipitation takes place in an intermediate zone. The outermost degraded zone consists of alumina and silica gels.

The coupling of (bio)chemical alteration, porosity and diffusion evolutions is a key step. The modeling accurateness of calcium leaching, pH evolution and degradation thickness has been enhanced in a consistent manner whilst considering increase of diffusivity in the degraded zones. Modeling has indicated that cement biodegradation is essentially driven by acidic hydrolysis and not by complexation. Nonetheless, aluminum complexation by acetate and oxalate may have an effect on the stability of the alumina gel layer that is formed in the degraded layer, or in the proportion of aluminum inserted into the silica gel. A massive precipitation of calcium oxalate has been predicted by modeling at the surface of the cement pastes but was in reality hindered in the bioleaching reactor.

This study has demonstrated that reactive transport models can be applied to assess durability and long-term performance of cement-based materials subjected to biodegradation. However, a set of improvement are still required. Complementary thermodynamic data are still needed (e.g. lactate complexes, aluminum salts) upstream of calculations. The calculated mineralogical fronts were too sharp compared to experiment, claiming for kinetics and/or heterogeneous modeling of the degradation front.

Acknowledgments

The constructive and detailed comments of the anonymous reviewers are gratefully acknowledged as well as our colleagues, Jan van der Lee and Vincent Lagneau, for their tremendous contributions to the development of HYTEC.

References

[1] M. Diercks, W. Sand, E. Bock, Microbial corrosion of concrete, Experientia 47 (1991) 514–516.
[2] J. Monteny, E. Vincke, A. Beeldens, N. De Belie, L. Taerwe, D. Van Gemert, W. Verstraete, Chemical, microbiological, and in situ test methods for biogenic sulfuric acid corrosion of concrete, Cem. Concr. Res. 30 (2000) 623–634.
[3] N. De Belie, H.J. Verselder, B. De Blaere, D.V. Nieuwenburg, R. Verschoore, Influence of the cement type on the resistance of concrete to feed acids, Cem. Concr. Res. 26 (1996) 1717–1725.
[4] A. Bertron, J. Duchesne, G. Escadeillas, Attack of cement pastes exposed to organic acids in manure, Cem. Concr. Comp. 27 (2005) 898–909.
[5] H. Lajili, P. Devillers, C. Grambin-Lapeyre, J.P. Bournazel, Alteration of a cement matrix subjected to biolixiviation test, Mater. Struct. 41 (2008) 1633–1645.
[6] J.D. Gu, T.E. Ford, N.S. Berke, R. Mitchell, Biodeterioration of concrete by the fungus *Fusarium*, Int. Biodeterior. Biodegrad. (1998) 101–109.
[7] C. Gaylarde, M. Ribas Silva, T. Warscheid, Microbial impact on building materials: an overview, Mater. Struct. 36 (2003) 342–352.
[8] A. Jestin, M. Libert, P. Thouvenot, R. Sellier, J.P. Bournazel, Biodégradation de matrices cimentaires, Rev. Europ. Génie Civil 8 (2004) 1087–1104.
[9] F. Adenot, M. Buil, Modelling of the corrosion of the cement paste by deionized water, Cem. Concr. Res. 22 (1992) 489–496.
[10] M. Mainguy, C. Tognazzi, J.M. Torrenti, F. Adenot, Modelling of leaching in pure cement paste and mortar, Cem. Concr. Res. 30 (2000) 83–90.
[11] K. Haga, S. Sutou, M. Hironaga, S. Tanaka, S. Nagasaki, Effect of porosity on leaching of Ca from hardened ordinary Portland cement paste, Cem. Concr. Res. 35 (2005) 1764–1775.
[12] S. Bejaoui, B. Bary, Modeling of the link between microstructure and effective diffusivity of cement pastes using a simplified composite model, Cem. Concr. Res. 37 (2007) 469–480.
[13] D. Sugiyama, T. Fujita, T. Chida, M. Tsukamoto, Alteration of fractured cementitious materials, Cem. Concr. Res. 37 (2007) 1257–1264.
[14] E. Stora, B. Bary, Q.C. He, E. Deville, P. Montarnal, Modelling and simulations of the chemo-mechanical behaviour of leached cement-based materials: leaching process and induced loss of stiffness, Cem. Concr. Res. 39 (2009) 763–772.
[15] M. Moranville, S. Kamali, E. Guillon, Physicochemical equilibria of cement-based materials in aggressive environments — experiment and modelling, Cem. Concr. Res. 34 (2004) 1569–1578.
[16] M.K. Wang, J.L. White, S.L. Hem, Influence of acetate, oxalate and citrate anions on precipitation of aluminum hydroxide, Clays Clay Miner. 31 (1983) 65–68.
[17] R.E. Beddoe, H.W. Dorner, Modelling acid attack on concrete: Part I. The essential mechanisms, Cem. Concr. Res. 35 (2005) 2333–2339.
[18] A. Bertron, S. Larreur-Cayol, T. Minh Hu, G. Escadeillas, Degradation of cementitious materials by some organic acids found in agroindustrial environments, in: M.G. Alexander, A. Bertron (Eds.), Concrete in Aggressive Aqueous Environments, Performance, Testing and Modeling, RILEM Proceedings, 63, 2009, pp. 96–107.
[19] J. van der Lee, L. De Windt, V. Lagneau, P. Goblet, Module-oriented modeling of reactive transport with HYTEC, Comput. Geosci. 29 (2003) 265–275.
[20] A. Ohshima, I. Matsui, N. Yuasa, Y. Henmi, A study of growth of fungus and algae on mortar, Trans. Jpn. Concr. Inst. 21 (1999) 173–178.
[21] J.D. Allison, D.S. Brown, K.J. Novo-Gradac, MINTEQA2/PRODEF2, a Geochemical Assessment Model for Environmental Systems: Version 3.0 User's Manual. EPA/600/3-91/021. U.S. EPA, Athens, GA, 30605, 1991.
[22] Hatches, Hatches-r10, Database for Radio Chemical Modelling. Tech. rep, NEA, 1991.
[23] J. Cama, J. Ganor, The effects of organic acids on the dissolution of silicate minerals: a case study of oxalate catalysis of kaolinite dissolution, Geochim. Cosmochim. Acta 70 (2006) 2191–2209.
[24] S.A. Stronach, F.P. Glasser, Modeling the impact of abundant geochemical components on phase stability and solubility of the $CaO–SiO_2–H_2O$ systems at 25 °C: Na^+, K^+, SO_4^{2-}, Cl^- and CO_3^{2-}, Adv. Cem. Res 9 (1997) 167–181.
[25] R. Perkins, C. Palmer, Solubility of ettringite ($Ca_6[Al(OH)_6]_2(SO_4)_3\cdot 26H_2O$) at 5–75 °C, Geochim. Cosmochim. Acta 63 (1999) 1969–1980.
[26] T. Wolery, EQ3/6. A software package for geochemical modelling of aqueous systems: package overview and installation guide (version 7.0). Technical Report UCRL-MA-110662 PT I ed. (1992), Lawrence Livermore National Laboratory, USA.
[27] D. Bennet, D. Read, M. Atkins, F. Glasser, A thermodynamic model for blended cements. II: Cement hydrate phases, thermodynamic values and modelling studies, J. Nucl. Mater. 190 (1992) 315–325.

[28] D. Damidot, F.P. Glasser, Thermodynamic investigation of the $CaO–Al_2O_3–CaSO_4–H_2O$ system at 25 °C and the influence of Na_2O, Cem. Concr. Res. 23 (1993) 221–238.
[29] S. Smillie, F.P. Glasser, Reaction of EDTA, oxalic and citric acid with Portland cement, Adv. Cem. Res 11 (1999) 97–101.
[30] L. De Windt, R. Badreddine, Modelling of long-term dynamic leaching tests applied to solidified/stabilised waste, Waste Manag. 27 (2007) 1638–1647.
[31] L. Trotignon, V. Devallois, H. Peycelon, C. Tiffreau, X. Bourbon, Predicting the long term durability of concrete engineered barriers in a geological repository for radioactive waste, Phys. Chem. Earth 32 (2007) 259–274.
[32] A. Bertron, J. Duchesne, G. Escadeillas, Accelerated tests of hardened cement pastes alteration by organic acids: analysis of the pH effect, Cem. Concr. Res. 35 (2005) 155–166.